Additive Manufacturing 66 (2023) 103456

Contents lists available at ScienceDirect

Additive Manufacturing

journal homepage: www.elsevier.com/locate/addma

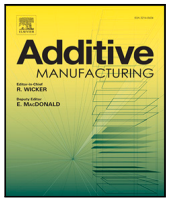

Research paper

Development of robot assisted hybrid additive manufacturing technology for the freeform fabrication of lattice structures

Anna De Marzi, Michele Vibrante, Matteo Bottin, Giorgia Franchin *

Department of Industrial Engineering, University of Padova, Padova 35131, Italy

ARTICLE INFO

Keywords:
Robot assisted
Hybrid
Direct ink writing
Photopolymerization
Lattice structures
Freeform

ABSTRACT

The extensive study and development of additive manufacturing technologies have allowed not only increased customization of the final parts but especially of their complexity. From such perspectives, intricate and mechanically efficient lattices which maximize their strength-to-weight ratio could be printed. Nevertheless, the fabrication of regular lattices, like octet cells, has been proven to be particularly limited by the layer-by-layer construction process due to the introduction of additional interfaces and/or the requirement of supports. In this work, a hybrid extrusion–photopolymerization process is coupled with a 6-axis robotic arm to allow for the fabrication of layers-less lattices thanks to the use of a custom graphical user interface and control over the printing head orientation. A highly reactive resin is employed as the ink and loaded with silica particles in order to tailor its rheological properties. A good resemblance between the printed components and the digital model is achieved, while their mechanical properties are superior to the ones of the traditionally additive manufactured octets.

1. Introduction

Lattices are a particular class of cellular solids characterized by the repetition of a regular pin-jointed frame made of trusses and surrounded by a void space [1]. A more rigorous classification of such structures can be done based on their connectivity and the consequence of such parameter in the deformation mechanism. Specifically, whereas low-connected lattices deform following a bending-dominated mechanism, high-connected lattices behave as stretch-dominated structures meaning that their trusses do not bend upon loading but only carry tension or compression [2]. Such mechanism for the distribution of stresses creates a rigid and un-foldable structure with a strength-to-weight ratio especially suitable for lightweight structural applications (i.e., aerospace, bio-engineering, and architecture) [3,4]. Typical representations of such configurations are tetrahedron and octahedron shapes [5]. Such regular lattices are intrinsically complex to fabricate using conventional manufacturing techniques (i.e., machining and molding), usually resulting in porous or defected objects [6]. Nevertheless, the rapid development of additive manufacturing (AM) technologies has opened new ways, allowing not only a fast and cost-efficient structure prototyping, due to their ability to selectively deposit material where it is needed, but especially an increase of the printable structure complexity [7]. However, using current AM techniques for the fabrication of lattices, such as Fused Filament Fabrication (FFF) or Digital Light Processing (DLP), generally requires the addition of support structures, sacrificial materials or long exposure times [8–10]. Moreover, AM technologies are layer-by-layer manufacturing methods thus intrinsically characterized by the presence of many interfaces between layers which leads to reduced strength and mechanical response of the printed parts [11,12].

Several approaches have proved able to overcome such phenomena, including the optimization of the part orientation and/or the use of a variable layer thickness. Nonetheless, such solutions are still based on a planar construction: the effect of the interfaces between layers is reduced but not removed, ultimately resulting in an increase of the overall processing time [13–15]. From such perspectives, it is clear that in order to control the trusses orientation and promote a better loading performance of the lattices, AM technologies not based on a layer-by-layer approach would represent the best solutions. Liu et al. using an FFF printer, for example, proved that it is possible to fabricate a lattice truss core without using any support thanks to a precise calibration of the extruder temperature and of the cooling system together with the modification of the free-hanging printing path [16]. Similarly, other solutions are represented by assisted or coupled processes resulting from the combination of two or more AM technologies within a single hybrid manufacturing technique [17]. An example is the UV-assisted Direct Ink Writing technology (UV-DIW) in which a photo-curable suspension is extruded through a nozzle and consequently cured enabling retention of its shape in thin air [18].

* Corresponding author.
E-mail address: giorgia.franchin@unipd.it (G. Franchin).

https://doi.org/10.1016/j.addma.2023.103456
Received 19 October 2022; Received in revised form 16 January 2023; Accepted 14 February 2023
Available online 21 February 2023
2214-8604/© 2023 Elsevier B.V. All rights reserved.

Nonetheless, such freeforming processes still rely on a 3-axis setup: the high degree of freedom given by the non-planar construction is limited by the collision of the printing head with the printed structure [19,20]. In addition, the angle between the nozzle and the deposition direction varies during the printing process, hence continuously changing the point of solidification and affecting the accuracy of the free-hanging structure [21–23]. In order to further overcome the aforementioned limits, a possible solution is to pair the described freeforming technologies to a robotic arm [24–27]. Due to the unlocking of additional axes, such techniques allow for the deposition of the material along the trusses direction, thus aligning the expected tension/compression forces with the struts and, therefore, maximizing the stiffness of the structure [28,29]. While the majority of the published works are based on FFF robot arm-assisted processes, few examples have been reported in the literature demonstrating the capabilities of the UV-DIW in a 6-axis environment [30–32]. Specifically, such works do not explore in depth the increased degree of freedom of the coupled technology: the UV curing only aids the material consolidation after layer-by-layer deposition, without exploring the fabrication of suspended trusses [31–33].

Here, the full potential of a UV-DIW setup coupled with a 6-axis robotic arm is exploited. A customized graphic interface is developed allowing control over the printing parameters and the robot relative positioning to the nozzle end. Regular octet lattices made of photocurable ink are fabricated. The freeform ability of the system is assessed by evaluating the ink rheology and curing behavior as well as the samples matching with the digital file. The enhanced mechanical properties of the fabricated lattices are tested through uni-axial compression and compared with layer-based lattices fabricated via DLP.

2. Materials and methods

2.1. Robot system setup for hybrid UV-DIW printing

The printing setup is schematized in Fig. 1 and shown in **Fig. SI 1**. It consists of a dispensing system – extruder (vipro-HEAD 3, ViscoTec Pumps and Dosing Technology GmbH, Germany) and UV-blocking nozzle tip (d = 0.84 mm, Vieweg GmbH, Germany) – installed as the end-effector on a 6-axis industrial robot (RV-4FRL-D, Mitsubishi Electric Corporation, Japan). The connection of the extruder to the robotic flange is possible through the use of an aluminum support. Such support has been designed so that the robot workspace is maximized. In fact, the encumbrance of the extruder makes it easy for the robot to collide with its own structure when tight movements are required by the task. In addition, to the aluminum support another structure is fixed, which is equipped with a set of six UV-LED chips (395-−400 nm, I=34 mW cm^{-2}, 3 Watt). Such UV-LED chips are evenly distributed and installed around the nozzle tip of the extruder by means of a custom 3D printed copper add-on (**Fig. SI 1**) which is placed on the structure to dissipate the heat generated by UV-LED chips.

The UV-LEDs work by curing within seconds the viscous photopolymer exiting from the nozzle during printing operations, obtaining in this way the hybrid UV-DIW technology. A syringe containing the material under gas pressure of 2 MPa feeds the extruder. The robot prints parts above an elevated non-reflective glass plate, in order to avoid non-homogeneous solidification of material caused by the reflected UV light from the plane.

2.2. Custom GUI

The fabrication of different components (examples of which are shown in **Fig. SI 2**) using the robot assisted hybrid additive manufacturing technology was enabled by the development of a custom Graphical User Interface (GUI), schematized in Fig. 2. Specifically, G-code files are the input data for the GUI: they contain information about the cartesian coordinates of the path, the printing speed, and the extrusion parameter (E), defining the deposition of the material along the cartesian path.

G-code files are then processed following two different paths. On one hand, the cartesian coordinates of the G-code file are converted, through a kinematic inversion process, in joint coordinates and sent as output to the software RT Toolbox 3 (Mitsubishi Electric Corporation, Japan), which controls the robot movements. On the other hand, a PLC (EK1100, Beckhoff Automation GmbH & Co. KG, Germany) is employed to control the switching of the module associated with the extruder (EL7370, Beckhoff Automation GmbH & Co. KG, Germany) and that of the UV-LEDs (EL2808, Beckhoff Automation GmbH & Co. KG, Germany).

These information are essential to simultaneously control the robot movements and the end-effector through the PLC, but they are not sufficient. Indeed, the kinematic of industrial robots, and in particular the one of anthropomorphic manipulators, requires information about translations, rotations, and configurations of the robotic arm to execute the kinematic inversion. The translation movements are provided by the cartesian coordinates of the G-code file; the robot configuration is defined by default as the one that maximizes the printing workspace volume (as shown in Section 3.1); on the other hand, the rotations that the nozzle tip assumes along the path during AM operations can either be manually set by the GUI user or automatically calculated by the GUI. In the first case, the orientation of the nozzle with respect to the vertical direction will be kept constant throughout all the printing process. This limits the high degree of freedom provided by the additional axes possessed by the robot arm compared to 3-axis AM techniques. In this sense, the GUI was customized in order to automatically calculate the inclination of the end-effector: the nozzle tip will be oriented in order to keep its axis always coincident with the direction of the G-code path. Considering the encumbrance of the end-effector and the optimization of the workspace, an angle of 60° with respect to the vertical direction was found as the maximum inclination capacity of the end-effector setup.

The E parameter is also fed through the G-code file, which represents the length of the truss to extrude. The GUI translates such parameters in the rotational speed of the extruder by using a multiplier which depends on the truss printing speed. For the different truss-based components shown in this work, the printing speed range was defined between 0.5 and 5 mm/s.

2.3. Nozzle calibration with vision system

In robot programming, the robot has to know the transformation between the reference frame of the nozzle and the robot flange. The nozzle reference frame is placed so that the z axis points out from the nozzle, aligned with its axis of symmetry, while x and y axis can be placed arbitrarily. Since the nozzle is manually substituted after each print, there may be discrepancies between the ideal nozzle reference frame and the real one. These discrepancies may result in incorrect robot positioning which results in printing defects.

In order to print with high accuracy, a vision system (**Fig. SI 3**) is employed to identify the nozzle position and orientation in the robot reference frame. The vision system consists of an Allied Vision Mako G-192B camera that points to a station composed of two back-light panels of plexiglass and a mirror, disposed like in **Fig. SI 3**. The mirror is placed in such a way that the camera can capture both the nozzle tip and its lateral reflection. The camera system is calibrated by means of reference chessboards, a method well-known in literature [34].

When the nozzle tip is positioned in front of the camera, the back-lighted panels produce a homogeneous light that increases the contrast between the nozzle tip and the background. The camera takes a picture of both the nozzle tip and its reflection in the mirror. The direct and reflected images of the nozzle are processed, and corrections of the tool reference frame are set in the controller by comparing the images with reference ones. Then, a fixed point robot motion is performed, and

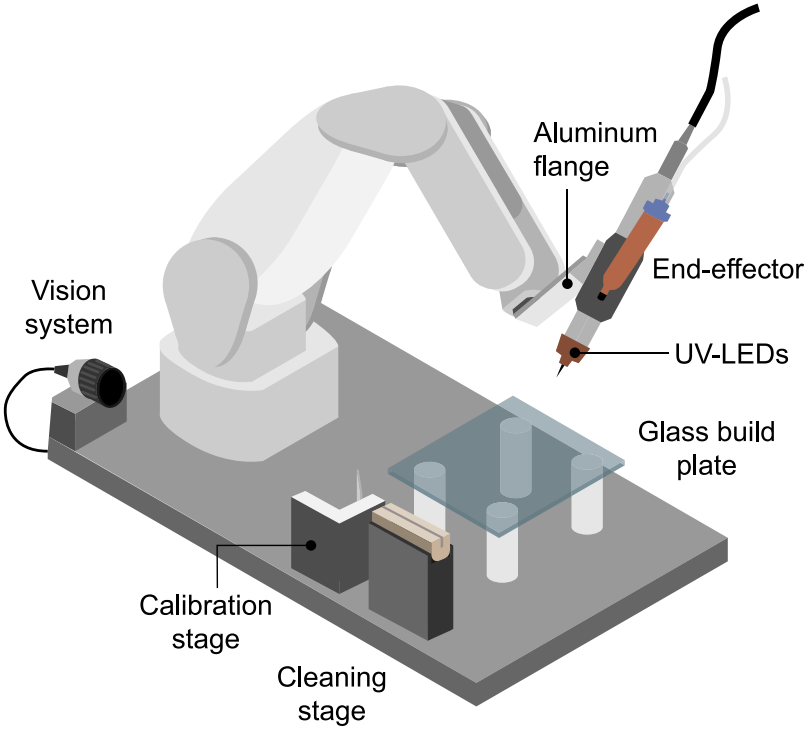

Fig. 1. Graphical representation of the robot hybrid UV-DIW setup.

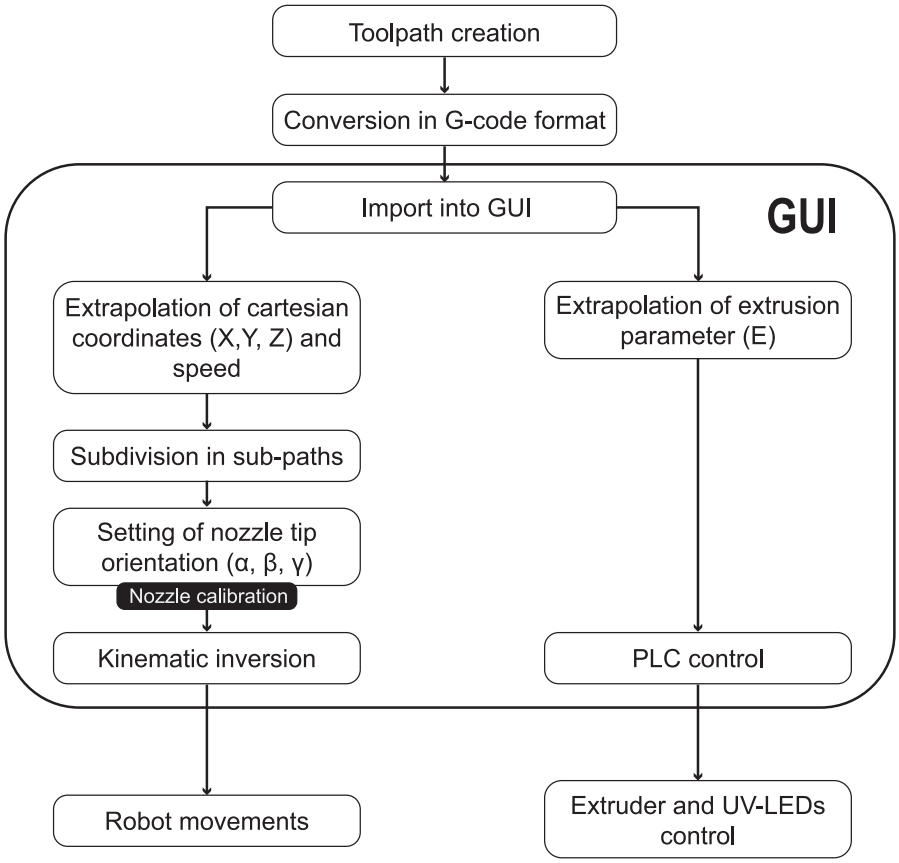

Fig. 2. Flow chart of the part production process using the GUI.

Table 1
Ink composition.

	wt%
Photocurable resin	90–95
Hydrophobic fumed silica	5–10

another photo is acquired, and new corrections of the tool reference frame are calculated. This process iterates until the nozzle tip is in the same position and orientation of a reference nozzle. By using this technique, x, y, and z coordinates can be calibrated, as well as the rotations around x, y, and z axes of the nozzle reference frame.

2.4. Ink preparation and characterization

The ink results from the addition of hydrophobic fumed silica treated with octamethylcyclotetrasiloxane (Aerosil® R 106, Evonik Industries AG, Germany) to a commercially available resin consisting in a mixture of acrylate and diacrylate monomers combined with a phosphine oxide based photoinitiator (Industrial Blend, FunToDo, Netherlands); 0.5 wt% of a coloring dye (E122, Squires Kitchen, England) in respect of the resin was also added to color the ink. Table 1 shows the ink composition.

Fumed silica and coloring dye were added to the resin followed by a mixing step of 6 min at 2000 rpm using a planetary mixer (ARE-250, THINKY, Japan), until complete dispersion. Once obtained, the ink was loaded into a syringe and later mixed using a defoaming step at 1200 rpm for 2 min to release the air entrapped during the loading procedure.

A rotational rheometer (Kinexus Lab+, Netzsch, Germany) equipped with a 1°/40 mm cone-plate geometry, with a gap of 0.03 mm, was employed to analyze the rheological behavior of the ink. The shear stress and viscosity were measured as a function of the shear rate in the interval of 1–1000 s^{-1}. A UV-plate system accessory (KNX5007, Netzsch, Germany) equipped with a 40 mW cm^{-2} UV lamp was employed for photo-rheological characterization using an 8 mm parallel plate geometry and a 0.5 mm gap. A three intervals thixotropy test (3ITT) was performed to follow the evolution of the shear viscosity: (i) 0.5% strain for 30 s at 1 Hz; (ii) 100 s^{-1} of shear rate for 30 s; (iii) 0.5% strain for 5 min at 1 Hz; during the last step, the UV light was switched on for different time intervals (0 s, 1 s).

The UV light intensity was measured with a UV power meter console (PM400, Thorlabs Inc., USA) coupled with a photodiode power sensor (S120VC, Thorlabs Inc., USA).

The curing depth of the suspension was determined with a micrometer screw gauge by measuring the thickness of the cured portion of ink droplets processed by the UV-LEDs at different exposure times. The corresponding energy densities were calculated as the product of intensity and exposure time.

2.5. Samples characterization

The comparison between the printed samples and the starting CAD model was done by using a Java-based image processing program (ImageJ, NIH, USA) [35]. The values were obtained by measuring the thickness and inclination of 4 struts from 10 different octet structures, for a total of 40 values each.

Fractographical analysis was carried out using an optical stereomicroscope (AxioCam ERc 5s Microscope Camera, Carl Zeiss Microscopy, Thornwood, USA) and scanning electron microscopy (Cube II, EmCrafts, Korea) at 10 kV and magnification of 500 X.

Mechanical properties of the printed octahedron geometries were tested in compression, using a universal testing machine (Quasar 25, Galdabini s.r.l., Italy) operating with a crosshead speed of 2 mm/min. Force vs. displacement curves of 6 different samples was compared with those obtained from octets fabricated using a DLP printer (Prusa SL1, Prusa Research, Czech Republic); layer thickness and exposure time were set to 100 μm and 2 s/layer, respectively.

3. Results and discussion

3.1. Robot calibration

The calibration method described in Section 2.3 has been tested with the experimental setup. After a calibration process, rotations around the three axes of the tool reference frame are performed, and the displacement errors of the tips with respect to the reference position are measured by means of the vision system. To assess the validity of the method, it has been compared with two other methods: the first one uses the transformation matrix between the robot flange and the tool reference frame retrieved by the CAD model, while the other uses the robot integrated calibration procedure, which is given by the proprietary software RT Toolbox.

Results are shown in Fig. 3 (a–c). The proposed calibration method is perfectly aligned with the other methods, while in some situations outperforms the existing solutions. However, the main advantages of the proposed method rely on two aspects: time savings and reduction of human errors. As mentioned, the calibration process must be performed each time a new nozzle is manually mounted at the end of the extruder. The RT Toolbox method requires manual robot movements which may take a very long time and is prone to errors. Instead, the proposed method is fully automated by means of the GUI program. Moreover, the CAD method does not consider the inevitable changes in the tool reference frame that are due to the different nozzle tightening forces. As per our tests, the proposed method has proved to be more reliable and less time-consuming for the operator.

Please note that the design of the end effector is prone to manufacturing errors in all 6 degrees of freedom of the tool transformation matrix (both displacements and rotations) since none of the tool reference frame axes is aligned with the robot axes [36]. This design is required since the extruder is particularly long, thus cannot be installed aligned with the robot 6-axis.

To optimize the setup design, an analysis of the workspace dimension has been performed. In such analysis, the target was to calculate each position of the entire robot workspace in which the robot could print with the nozzle placed within a vertical cone with a maximum angle of 60° with respect to the vertical axis; in other words, every position of the workspace in which the robot can incline the nozzle up to 60° with respect to the vertical axis and rotate around the vertical axis about 360°. Both joint mechanical limits and collision with the workcell equipment have been considered.

In Fig. 3(d) examples of valid configurations are shown where the nozzle inclination with respect to the vertical axis is either +60° or −60°. Each configuration can only reach specific positions; their intersection, i.e. the central volume in the graph, defines the valid workspace of the setup. Within this space, the printing volume can be placed according to the needs. Note that the tool has been designed so that the nozzle tip is inclined by 45° with respect to the last joint axis. In fact, the workspace volume with such an angle is around 6800 cm^3, while a nozzle tip aligned with the last joint axis would allow a workspace of around 1000 cm^3. Moreover, we decided to use a raised platform (Fig. 1) in order to prioritize the printing area rather than the height.

3.2. Freeform ability of the ink

As described, the UV-DIW printing process derives from the coupling of the DIW technique with an external UV source: the printing parameters usually associated with the extrusion processes (i.e., printing speed and flow rate), had to be tailored considering also the polymerization mechanism of the ink. Specifically, a suitable ink for the UV-DIW process is represented by a highly reactive photo-curable paste possessing sufficient viscosity to allow for a stable flow out of the nozzle and a flow rate than can be matched by the curing rate of the system [23]. Here, a commercially available acrylate-based resin was

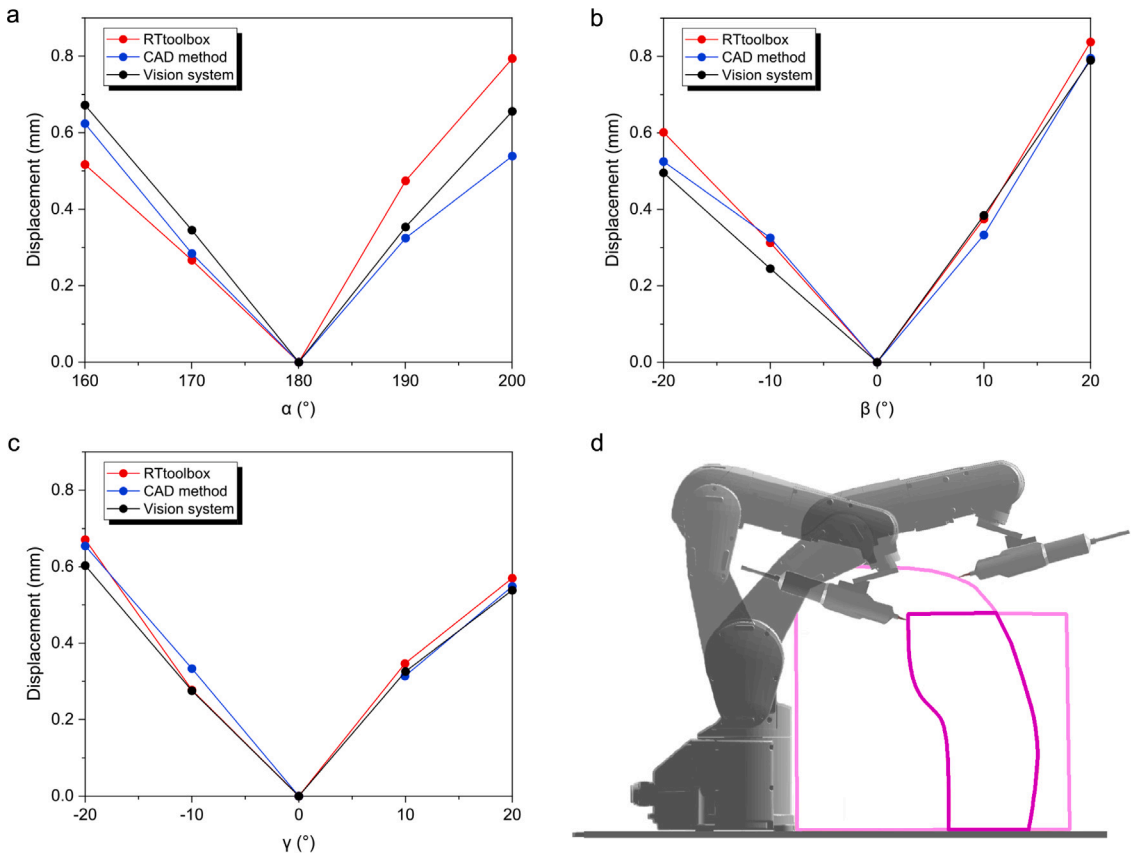

Fig. 3. Displacement of the nozzle tip with respect to the reference position during the rotation around the three axes of the reference frame: α (a), β (b), γ (c). Valid robot configurations with the nozzle inclined of +60° (right) and −60° (left) with respect to the vertical axis. The overall valid workspace is the intersection of the two volumes (pink) (d). (For interpretation of the references to color in this figure legend, the reader is referred to the web version of this article.)

selected as the reactive phase: its composition makes it suitable to be rapidly cured upon exposition to UV light [37]. Nonetheless, such resin displays a nearly constant viscosity of 0.14 Pa s, shown in Fig. 4(a), which does not meet the process requirements.

Therefore, in order to tailor its rheological behavior, the resin was loaded with different fractions of fumed silica particles. As expected, an increase in the value of the solid loading – from 5 wt% to 10 wt% – results in the gradual increase of the ink viscosity; there is also a gradual shift from a Newtonian to a shear-thinning behavior, which aids in preventing the sagging of the extruded filament prior to its curing [18]. The ink with 10 wt% loading was selected as it matches the behavior of a previously published printable ink [23].

The critical energy dose required to start the polymerization process can be calculated using the Jacobs equation [38]:

$$C_d = D_p \cdot ln(E/E_c) \tag{1}$$

where C_d (mm) is the curing depth at given exposure time, E is the energy density at the filament surface, E_cc is the critical energy dose and D_pp (mm) is the penetration depth of the ink [38]. Curing depth values of the ink were measured as a function of the energy density, as reported in Fig. 4(b). By following Eq. (1), the fitting of the experimental values returns the characteristics parameters of the ink: D_pp = 0.19 ±0.02mm and E_cc = 1.7 ±0.6 mJ cm^{-2} (R^2 = 0.95). Hence, a filament having a diameter of 0.84 mm would require only 0.46 s to fully cure upon radial exposition to UV light (C_dd = 0.42 mm, E = 15.5 mJ cm^{-2}, I = 34 mW cm^{-2}), suggesting a rapid retention of the filament after extrusion. This is despite the addition of the coloring dye – acting as photo absorber of the UV light – which was introduced only to create a visible contrast between the building plate and the trusses during the printing process.

The freeform ability of the ink was verified by assessing its behavior upon curing; therefore, the printing process was simulated through a three intervals thixotropy test (3ITT). Specifically, the three phases of the test correspond to (i) the ink at rest inside the syringe, before extrusion, (ii) the extrusion of the ink through the nozzle, and (iii) the ink status after extrusion. In Fig. 4(c) the 3ITT is reported for two different scenarios: a conventional DIW printing process with no UV light (black line), and the hybrid printing process with UV light switched on during the third interval for 1 s irradiation time (red line). As shown, if no UV light is present after extrusion, the ink takes a long time (> 20 s) to regain its initial viscosity; on the other hand, when the ink is UV-cured, there is a rapid increase of viscosity (3 orders of magnitude higher than its initial status). This suggests that a rigid cured filament can rapidly retain its shape after extrusion, thus validating its freeform ability.

3.3. Lattices fabrication

Octet lattices (**Fig. SI 4**) were designed having a unit cell length of 10 mm and thickness of 0.84 mm – corresponding to the diameter of the nozzle – therefore resulting in a theoretical aspect ratio ν equal to 0.084 ($\nu = \phi/L$). Whereas higher aspect ratios are usually desired in order to increase the final stiffness of the lattices [39], structures possessing low values of ν result in a higher energy absorption [40], making them particularly useful for lightweight and dynamic load conditions.

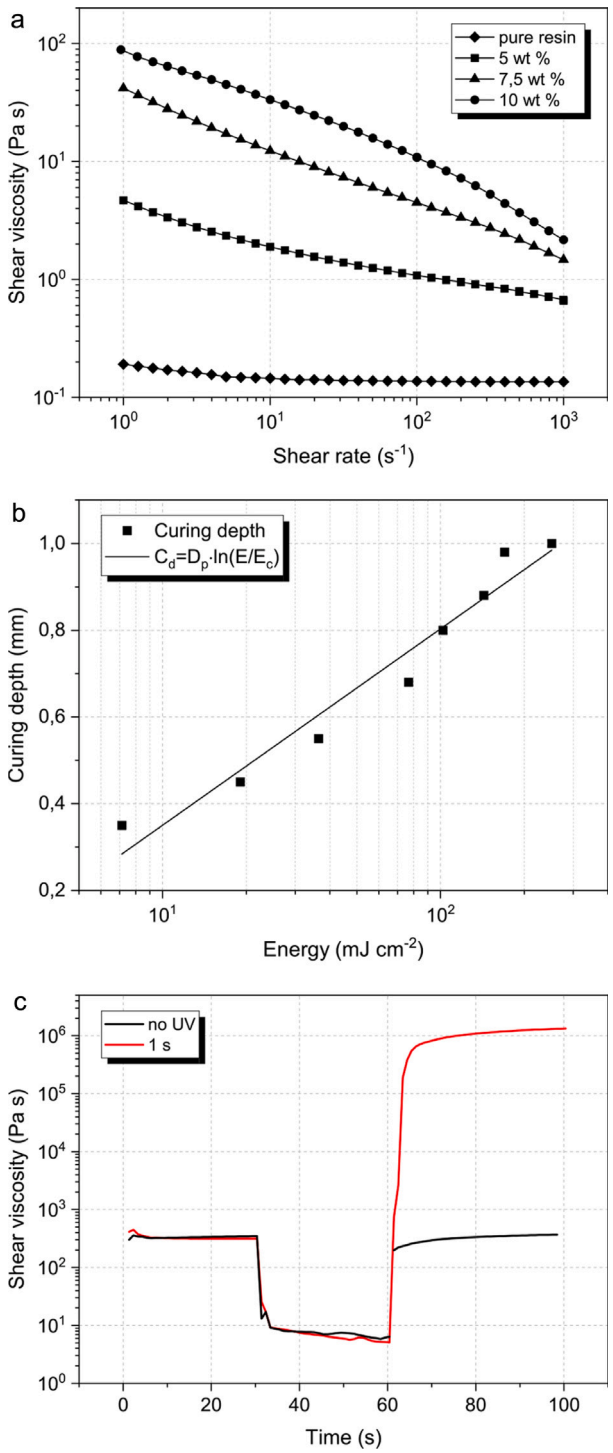

Fig. 4. Effect of the amount of silica on the (a) viscosity profile; (b) curing depth of the ink as a function of exposure energy density (logarithmic scale); (c) comparison of the three intervals thixotropy test (3ITT) on the 10wt% ink exposed to UV light (1 s) and not exposed (no UV).

Fig. 5(a) displays the obtained octet printed using the hybrid UV-DIW technique coupled with the custom GUI. As depicted in Fig. 6 and shown in **Video S 1**, the construction of the part is characterized by a discontinuous deposition of ink forming the trusses. Initially, the robot moves so that the tip of the extruder gets near the initial point; once in its proximity, the extruder approaches it by keeping its axis coincident with the direction of the to-be-printed truss (1). As the extrusion starting point is reached, ink is pre-extruded for a certain time (s), thus assuring the adhesion of the new truss to the platform or previously printed part (2). After that, the filament is extruded while moving at a certain printing speed and with the UV light switched ON (3); at the end of this phase, an extra UV exposure time (s) can be scheduled during which the extruder is not moving and does not extrude additional material (4). It was found empirically that the post-curing time is linearly proportional to the printing speed with a factor of about 4 (i.e., if the printing speed is 1 mm/s, the post-curing time is 4 s). After that, the filament is rigid enough to support itself, UV light is switched OFF and the extruder departs keeping its former direction (5). Finally, after moving away from the filament, the extruder travels again either to continue the construction of the next truss (6) or to the nozzle cleaning stage (**Video S 2**).

Thanks to the selective customization of the printing process parameters, each of the 36 trusses composing the octet could be fabricated using different orientations of the printing head, printing speed, and nozzle cleaning options. In particular, preliminary experiments highlighted frequent clogging and extrusion imperfections during the printing process, thus leading to the accumulation of cured material around the nozzle end and consequently influencing the deposition of the next trusses. Therefore, the technology setup was provided with a cleaning nozzle tip station, ultimately resulting in a reduction of material waste and an increase in printing repeatability. In addition to that, it was demonstrated how slower printing speeds are usually best for support-less features – since it means an increased energy dose in the same point – thus assuring a faster increase of the ink rigidity [22]. For the octet structure shown here (Fig. 5(a)), 0.85 mm/s speed and an angle of 35° of the printing head with respect to the vertical direction were selected to avoid collision with the rest of the printed structure. There is a quite good resemblance with the digital model; struts possess a thickness of 0.96 ± 0.06 mm and they are oriented at an angle of 44.5 ± 0.5° in the front view. The noticeable discrepancy between the measured and modeled strut thickness (i.e., 0.84 mm), suggests a slight mismatch of the extruder speed with the printing one, as well as swelling associated with polymer extrusion [41]. On the other hand, the inclination of the struts reflects the designed one (i.e., 45°) in all directions. When compared to our previously published work [23], this is only deemed possible by the increased degree of freedom provided by the robot arm: thanks to the custom-developed GUI, it is possible to tilt the printing head and orient it along the truss axes, consequently avoiding the partial hindrance of the extruded filament by the nozzle and allowing for precise shape retention along the defined printing paths.

3.4. Effect of manufacturing method on the mechanical properties

As previously discussed, thanks to the optimal orientation of the printing head with respect to the printing path, it is possible to fabricate components in a non-planar fashion. Therefore, failure mechanisms associated with the stress evolution promoted by interlaminar interfaces in layer-wise produced components can be avoided [42,43].

In order to verify such hypotheses, the mechanical properties of octet lattices printed employing the presented hybrid UV-DIW technique were compared to ones fabricated using a DLP printer (Fig. 5(b)). It should be noted that DLP octets were fabricated using the less loaded ink (5 wt%). In fact, only inks with lower viscosity (i.e., below 5 Pa s) could be processed (i.e., easily and quickly cured) [44]. The effect of a 5 wt% increase in the silica content on the elastic modulus of a polymer nanocomposite is expected to be only marginal [45]. On the other hand, it can have a larger influence on its tensile strength: in similar materials, depending on the polymer matrix, the strength is shown to increase by about 12% to 24% when the silica content increases from 5 wt% to 10 wt% [46]. **Fig. SI 6** shows the compressive behavior of the two lattices. As expected, both structures behave as cellular solids: as the displacement increases, a first peak in the load (i.e., collapsing

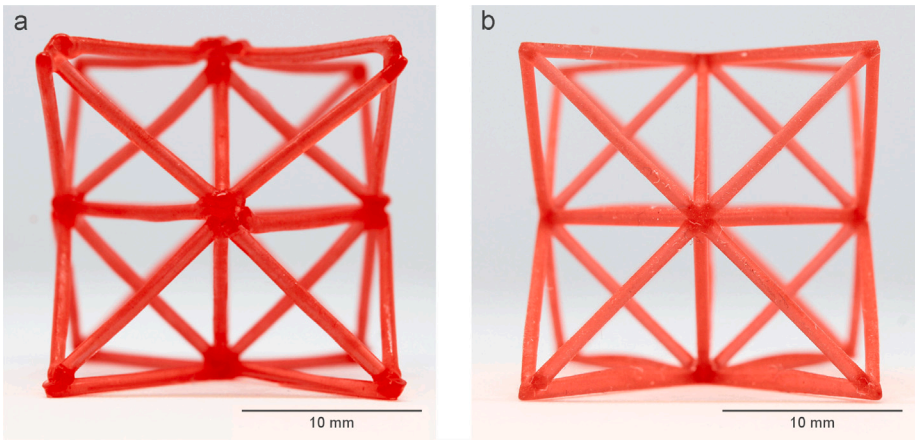

Fig. 5. Printed octet lattices; (a) via hybrid UV-DIW; (b) via DLP.

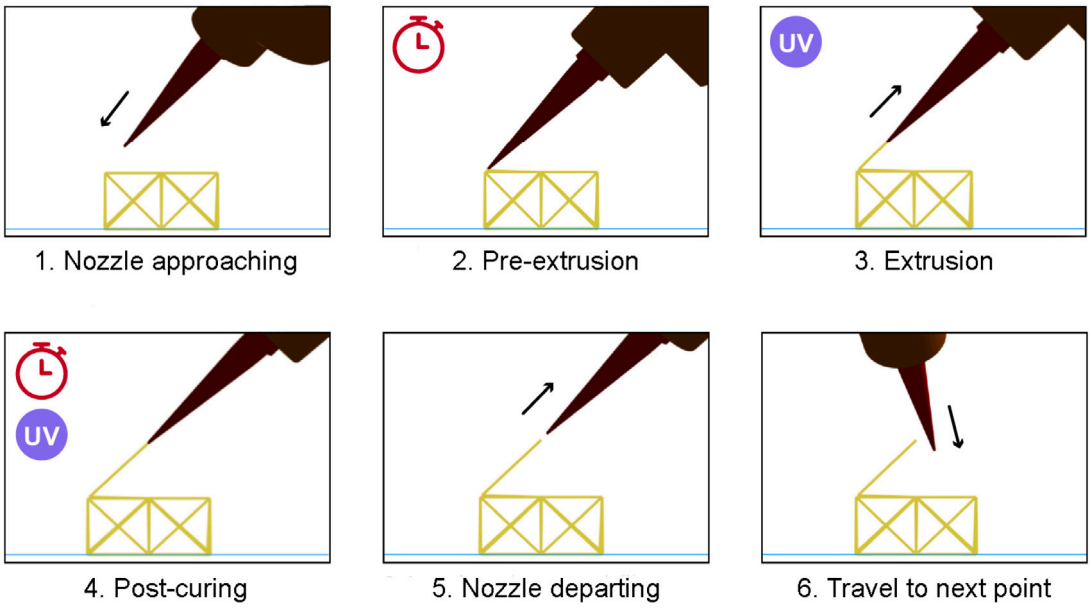

Fig. 6. Production part phases.

load) is reached, denoting the elastic region. Afterward, lattices enter the yielding phase, characterized by a fluctuation of the load value; this depends on the buckling, collapsing and re-distribution of the applied compression force to adjacent integer struts. Finally, there is a rapid increase in the load due to the compression of the material between the testing machine plates [5].

As a further confirmation of their cellular-like behavior, the failure mechanism of the two structures is observed; Fig. 7 indeed shows that both octets collapse by a gradual failure of the singular cells, moving from the one close to the moving plate through the static one [47]. However, differences between the two collapsing values can be noticed which should be attributed to the different manufacturing methods employed. Specifically, structures obtained via DLP display a collapsing value lower by 1 order of magnitude (i.e., 1.5 ± 0.3 N) compared to the one showed by octets printed via the hybrid technique (i.e., 17.5 ± 3.7 N). This can be attributed to two different mechanisms. The first one depends on the hybrid UV-DIW production process: in order to guarantee the connection between a new extruded truss and the already printed part, a pre-extrusion stage is performed at the beginning of each of the filaments. As a consequence, a higher amount of ink is accumulated in the nodes – as visible in **Fig. SI 5** – thus leading to an increase of the rigidity of the final component [27,48]. Differently, DLP structures are printed by the subsequent curing of the slices composing the CAD model. As depicted in Fig. 5(b), such a method allows for the fabrication of quite precise structures, thanks to the higher resolution of the DLP printer compared to the robot assisted UV-DIW, which consequently avoids the broadening of the node zones. In order to assess the impact of the nodes on the mechanical behavior, the CAD model employed for DLP was modified to mimick the robot pre-extrusion by adding spheres with a 0.9 mm diameter at the starting point of each of the trusses (**Fig. SI 7**(a)). The corresponding compressive behavior is reported in **Fig. SI 7**(b). As expected, the accumulation of ink at the nodes results in an increment of the strength to 8.0 ± 1.2 N; nonetheless, even considering the effect of a higher silica content, it remains significantly lower than that of octets printed with the hybrid UV-DIW technique.

The difference is therefore inputed to a second, more important mechanism, related to the presence of interlayer interfaces which characterizes all conventional AM techniques, including DLP. Specifically, the layer-by-layer construction introduces an additional roughness on the surface of the trusses, thus reducing their quality and ultimately creating new stress concentration points for cracks propagation [49,50]. This is highlighted in **Fig. SI 8(a-b)**, which shows one of the 45° inclined trusses of the DLP-octet; the crack initiated from the interface

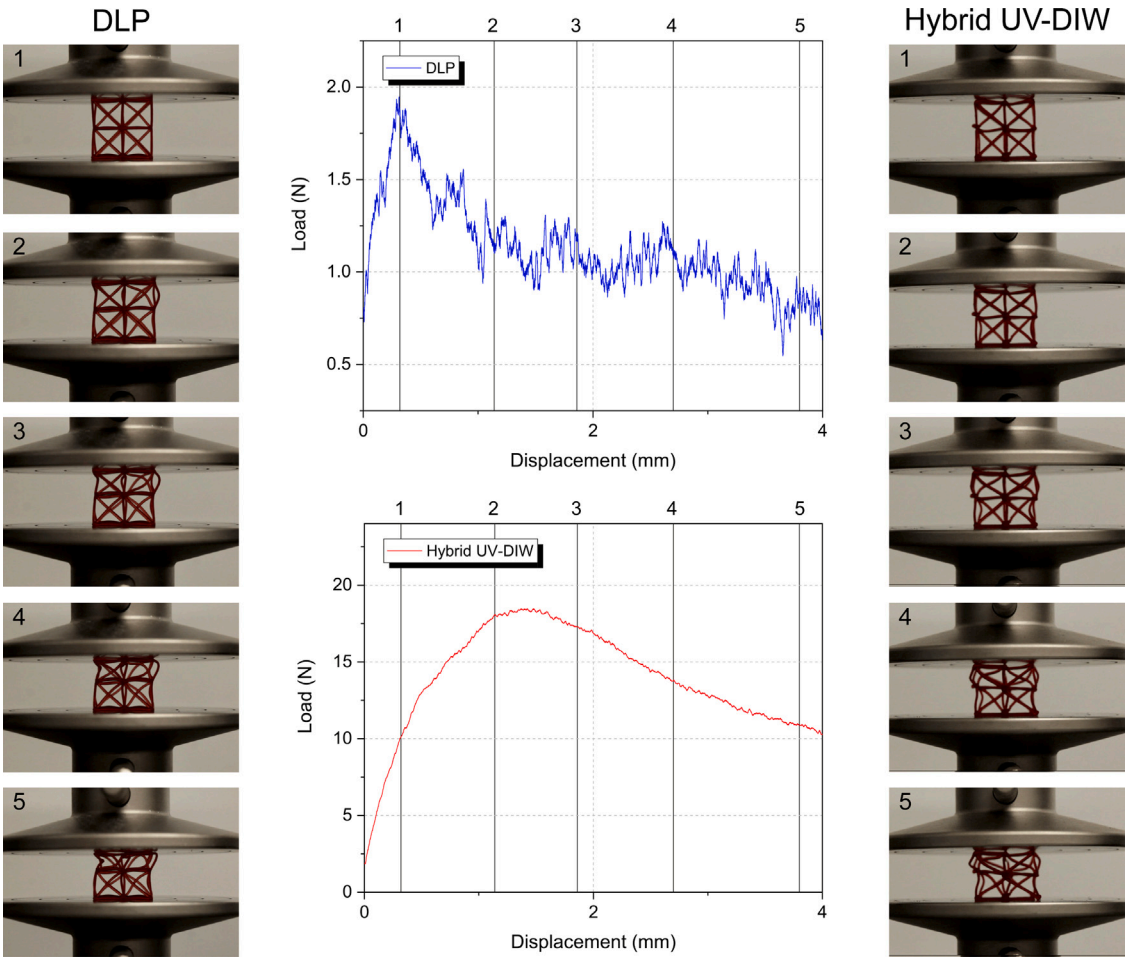

Fig. 7. Comparison of the failure mechanism of octet fabricated using a DLP printer and the hybrid UV-DIW setup by means of video frames and their corresponding moment in the compressive curves.

between two adjacent layers and resulted in the final rupture of the truss perpendicular to the printing direction. SEM investigation of the filament in proximity of the fracture surface **Fig. SI 8(c)** confirms this finding and also shows crack formation at several other interfaces.

A wide range of collapsing values is displayed by the hybrid printed structures (Fig. 6(a)); this can be attributed to errors associated with the robot arm setup. As previously discussed, while the setup design was chosen in order to maximize the workspace, its off-axis position lowers the precision of the last joint movements. The nozzle position can be misplaced up to its diameter size (as shown in Fig. 3), introducing systematic errors which are compensated manually by locally adapting the printing parameters (i.e., change of pre-extrusion time, phase 3 in Fig. 6). To further improve the robot accuracy, the entire workspace should be calibrated [51], which is not suitable for the proposed application, both in terms of equipment cost and time effort required.

4. Conclusions

In summary, the full potential of the UV-DIW technique coupled with a 6-axis robotic arm was exploited for the fabrication of regular octet lattice structures. A custom GUI was developed in order to selectively orient the printing head with the truss direction, thus promoting fast curing of the ink and increasing the accuracy of the printed part in comparison with the digital model. A better printing resolution could be achieved using a DLP process. Nevertheless, such technology requires a much longer time to fabricate the same structure (i.e., 45% more), more material to fill the printing vat, and an unavoidable cleaning step in order to remove excess material. In addition, its layer-wise approach ends up introducing interlayer interfaces inside of the trusses, thus not only negatively affecting the surface quality but especially the mechanical response of the octet structure. Indeed, in the lattices fabricated using the hybrid technique, the absence of interfaces, together with the creation of enlarged nodes, ultimately results in an increase in their strength as well as their energy absorption capabilities.

On the other hand, poorer accuracy was observed. In this sense, the most optimal configuration for the hybrid UV-DIW setup would be reached by aligning the axis of the extruder with that of the last joint of the robot arm. Such adjustment, however, would result not only in a smaller workspace but especially in a smaller range of inclination reachable by the printing head, thus downsizing the freeform ability of the hybrid setup.

Future work will include the further advancement of the hybrid setup capabilities by fabricating lattice structures using different materials; indeed, the poor transmittance of UV light and/or absorption phenomena that might be generated from the particles-light interaction have been proven to not be an issue for the technology [23]. In this sense, the combination of the mechanical properties of ceramic materials could be coupled together with the enhanced mechanical response of complex, stretch-dominated structures printed using the robot assisted UV-DIW setup.

CRediT authorship contribution statement

Anna De Marzi: Writing – original draft, Visualization, Validation, Investigation, Formal analysis, Data curation. **Michele Vibrante:** Writing – original draft, Validation, Software, Methodology, Investigation, Formal analysis, Data curation. **Matteo Bottin:** Writing – review & editing, Validation, Supervision, Methodology. **Giorgia Franchin:** Writing – review & editing, Validation, Supervision, Methodology, Conceptualization.

Declaration of competing interest

The authors declare that they have no known competing financial interests or personal relationships that could have appeared to influence the work reported in this paper.

Data availability

Data will be made available on request.

Acknowledgments

This research was partially funded by the Department of Industrial Engineering, University of Padova, Italy (project SID2020 "Hybrid Freeforming Extrusion - UV Assisted Additive Manufacturing Methods for the Fabrication of Ceramic Components with High Complexity"). The authors thankfully acknowledge Prof. Paolo Colombo and Prof. Giulio Rosati (University of Padova, Italy) for sharing their resources and insightful advice.

Appendix A. Supplementary data

Supplementary material related to this article can be found online at https://doi.org/10.1016/j.addma.2023.103456. Supplementary data include videos of the process, pictures of the setup and of printed components, details of the mechanical tests.

References

[1] L.J. Gibson, Cellular solids, Cambridge University Press, 1997, http://dx.doi.org/10.1017/CBO9781139878326.
[2] J.C. Maxwell, XLV. On reciprocal figures and diagrams of forces, Lond. Edinb. Dublin Philos. Mag. J. Sci. 27 (1864) 250–261, http://dx.doi.org/10.1080/14786446408643663.
[3] G.W. Kooistra, V.S. Deshpande, H.N.G. Wadley, Compressive behavior of age hardenable tetrahedral lattice truss structures made from aluminium, Acta Mater. 52 (14) (2004) 4229–4237, http://dx.doi.org/10.1016/j.actamat.2004.05.039.
[4] V.V. Vasiliev, A.F. Razin, Anisogrid composite lattice structures for spacecraft and aircraft applications, Compos. Struct. 76 (1–2) (2006) 182–189, http://dx.doi.org/10.1016/j.compstruct.2006.06.025.
[5] P. Colombo, M. Scheffler, Cellular Ceramics, WILEY-VCH Verlag GmbH & Co. KGaA, Weinheim, 2005.
[6] C.T. Richard, T.-H. Kwok, Analysis and design of lattice structures for rapid-investment casting, Materials 14 (2021) 4867–4888, http://dx.doi.org/10.3390/ma14174867.
[7] H. Cui, R. Hensleigh, D. Yao, D. Maurya, P. Kumar, M.G. Kang, S. Priya, X.R. Zheng, Three-dimensional printing of piezoelectric materials with designed anisotropy and directional response, Nature Mater. 18 (2019) 234–241, http://dx.doi.org/10.1038/s41563-018-0268-1.
[8] A.T. Gaynor, J.K. Guest, Topology optimization considering overhang constraints: Eliminating sacrificial support material in additive manufacturing through design, Struct. Multidiscip. Optim. 54 (2016) 1157–1172, http://dx.doi.org/10.1007/s00158-016-1551-x.
[9] C.S. O'Bryan, T. Bhattacharjee, S.R. Niemi, S. Balachandar, S.T.E. Nicholas Baldwin, C.R. Taylor, W.G. Sawyer, T.E. Angelini, Three.dimensional printing with sacrificial materials for soft matter manufacturing, 3D Bioprint. Organs 42 (2017) 571–577, http://dx.doi.org/10.1557/mrs.2017.167.
[10] P. Yin, L. Yi, C. Xiao, X. Cao, L. Zhao, H. Shi, Engineering of removing sacrificial materials in 3D-printed microfluidics, Micromachines 9 (7) (2018) 327, http://dx.doi.org/10.3390/mi9070327.
[11] M.R. Karamooz Ravari, M. Kadkhodaei, M. Badrossamay, R. Rezaei, Numerical investigation on mechanical properties of cellular lattice structures fabricated by fuse deposition modelling, Int. J. Mech. Sci. 88 (2014) 154–161, http://dx.doi.org/10.1016/j.ijmecsci.2014.08.009.
[12] X. Wang, Y. Zhou, L. Zhou, X. Xu, S. Niu, X. Li, X. Chen, Microstructure and properties evolution of silicon-based ceramic cores fabricated by 3D printing with stair-stepping effect control, J. Eur. Ceramic Soc. 41 (8) (2021) 4650–4657, http://dx.doi.org/10.1016/j.jeurceramsoc.2021.03.036.
[13] K.S. Bhole, B. Kale, Techniques to minimise stair-stepping effect in micro-stereolithography process: A Review, Adv. Mater. Proces. Technol. (2021) 1–20, http://dx.doi.org/10.1080/2374068X.2021.1970997.
[14] M. Taufik, P.K. Jain, Role of build orientation in layered manufacturing: a review, Int. J. Manufact. Technol. Manage. 27 (2014) 1–3, http://dx.doi.org/10.1504/IJMTM.2013.058637.
[15] R.L. Hope, R.N. Roth, P.A. Jacobs, Adaptive slicing with sloping layer surfaces, Rapid Prototyp. J. 3 (3) (1997) 89–98, http://dx.doi.org/10.1108/13552549710185662.
[16] S. Liu, Y. Li, N. Li, A novel free-hanging 3D printing method for continuous carbon fiber reinfotced thermoplastic lattice truss core structures, Mater. Des. 137 (2018) 235–244, http://dx.doi.org/10.1016/j.matdes.2017.10.007.
[17] M. Merklein, D. Junker, A. Schaub, F. Neubauer, Hybrid additive manufacturing technologies, Physics Procedia 83 (2016) 549–559, http://dx.doi.org/10.1016/j.phpro.2016.08.057.
[18] L.L. Lebel, B. Aissa, M.A.E. Khakani, D. Therriault, Ultraviolet-assisted direct-write fabrication of carbon nanotube/polymer nanocomposite microcoils, Adv. Mater. 22 (2010) 592–596, http://dx.doi.org/10.1002/adma.200902192.
[19] S. Mueller, S. Im, S. Gurevich, A. Teibrich, L. Pfisterer, F. Guimbretiere, P. Baudisch, WirePrint: 3D printed previews for fast prototyping, in: UIST '14: Proceedings of the 27th Annual ACM Symposium on User Interface Software and Technology, 2014, http://dx.doi.org/10.1145/2642918.2647359.
[20] Y. Jin, J. Du, Y. He, G. Fu, Modeling and process planning for curved layer fused deposition, Int. J. Adv. Manuf. Technol. 91 (2017) 273–285, http://dx.doi.org/10.1007/s00170-016-9743-5.
[21] M. Eichenhofer, J.C.H. Wong, P. Ermanni, Continuous lattice fabrication of ultra-lightweight composite structures, Addit. Manuf. 18 (2017) 48–57, http://dx.doi.org/10.1016/j.addma.2017.08.013.
[22] R.D. Farahani, L.L. Lebel, D. Therriault, Processing parameters investigation for the fabrication of self-supported and freeform polymeric microstuctures using ultraviolet-assisted three-dimensional printing, J. Micromech. Microeng. (2014) 1–12, http://dx.doi.org/10.1088/0960-1317/24/5/055020.
[23] A. De Marzi, G. Giometti, J. Erler, P. Colombo, G. Franchin, Hybrid additive manufacturing for the fabrication of freeform transparent silica glass components, Addit. Manuf. 54 (2022) http://dx.doi.org/10.1016/j.addma.2022.102727.
[24] I. Ishak, P. Larochelle, Robot arm platform for additive manufacturing: 3D lattice structures, in: 30th Florida Conference on Recent Advances in Robotics (FCRAR 2017), Miami, Florida, 2017.
[25] L. de Guevara, L.B. Manuel, J. Ficca, D. Byrne, R. Krishnamurti, Robotic free-oriented additive manufacturing technique for thermoplastic lattice and cellular structures, in: 24th International Conference of the Association for the Computer-Aided Architectural Design Research in Asia, CAADRIA, Hong Kong, 2019, http://dx.doi.org/10.52842/conf.caadria.2019.2.333.
[26] Y. Huang, Y. Xue, X. Wang, F. Han, Mechanical behavior of three-dimensional pyramidal aluminium lattice materials, Mater. Sci. Eng. A 696 (2017) 520–528, http://dx.doi.org/10.1016/j.msea.2017.04.053.
[27] K.-M.M. Tam, D.J. Marshall, M. Gu, J. Kim, Y. Huang, J. Lavalee, C.T. Mueller, Fabrication-aware structural optimisation of lattice additive-manufactured with robot-arm, Int. J. Rapid Manuf. 7 (2018) 120–168, http://dx.doi.org/10.1504/IJRAPIDM.2018.092908.
[28] K.-M.M. Tam, C.T. Mueller, Additive manufacturing along principal stress lines, 3D Print. Additive Manuf. 4 (2) (2017) http://dx.doi.org/10.1089/3dp.2017.0001.
[29] L. Li, A. Haghighi, Y. Yang, A novel 6-axis hybrid additive-subtractive manufacturing process: Design and case studies, J. Manuf. Process. 33 (2018) 150–160, http://dx.doi.org/10.1016/j.jmapro.2018.05.008.
[30] M. Asif, J.H. Lee, M.J. Lin-Yip, S. Chiang, A. Levaslot, T. Giffney, M. Ramezani, K.C. Aw, A new photoplomyer extrusion 5-axis 3D printer, Addit. Manuf. 23 (2018) 355–361, http://dx.doi.org/10.1016/j.addma.2018.08.026.
[31] X. Li, Q. Lian, D. Li, H. Xin, S. Jia, Development of a robotic arm based hydrogel additive manufacturing system for in-situ printing, Appl. Sci. 7 (73) (2017) 1–10, http://dx.doi.org/10.3390/app7010073.
[32] L. Velazquez, G. Palardy, C. Barbalata, Design and integration of end-effector for 3D printing of novel UV-curable shape memory polymers with a collaborative robotic system, in: Proceedings of CAMX 2021, Dallas, TX, 2021, http://dx.doi.org/10.48550/arXiv.2108.10810.
[33] A. Nicali, G. Pradal, G. Brandolini, A. Mantelli, M. Levi, Novel 3D printing method to reinforce implant-supported denture fiberglass as material for implant prosthesis: A pilot study, Clin. Exp. Dent. Res. (2022) http://dx.doi.org/10.1002/cre2.568.
[34] Z. Zhang, A flexible new technique for camera calibration, IEEE Trans. Pattern Anal. Mach. Intell. 22 (11) (2000) 1330–1334, http://dx.doi.org/10.1109/34.888718.
[35] C. Schneider, W. Rasband, K. Eliceiri, NIH Image to ImageJ: 25 years of image analysis, Nature Methods 9 (2012) 671–675, http://dx.doi.org/10.1038/nmeth.2089.
[36] M. Bottin, G. Rosati, Trajectory optimization of a redundant serial robot using cartesian via points and kinematic decoupling, Robotics 8 (4) (2019) http://dx.doi.org/10.3390/ROBOTICS8040101.

[37] C. Paredes, F.J. Martínez-Vázquez, H. Elsayed, P. Colombo, A. Pajares, P. Miranda, Evaluation of direct light processing for the fabrication of bioactive ceramic scaffolds: Effect of pore/strut size on manufacturability and mechanical performance, J. Eur. Ceram. Soc. 41 (2021) 892–900, http://dx.doi.org/10.1016/j.jeurceramsoc.2020.09.002.
[38] P.F. Jacobs, Rapid Prototyping & Manufacturing: Fundamentals of Stereolithography, Society of Manufacturing Engineers, 1992.
[39] P. Płatek, J. Sienkiewicz, J. Janiszewski, F. Jiang, Investigations on mechanical properties of lattice structures with different values of relative density made from 316l by selective laser melting (SLM), Materials 13 (9) (2020) 2204, http://dx.doi.org/10.3390/ma13092204.
[40] R. Guerra Silva, C. Salinas Estay, G. Morales Pavez, J. Zahr Viñuela, M.J. Torres, Influence of geometric and manufacturing parameters on the compressive behavior of 3d printed polymer lattice structures, Materials 14 (6) (2021) 1462, http://dx.doi.org/10.3390/ma14061462.
[41] K. Wang, Die swell of complex polymeric systems, Viscoelast. Theory Biol. Appl. 1 (2012) 77–96, http://dx.doi.org/10.5772/50137.
[42] J. Liu, J. Yan, H. Yu, Stress-constrained topology optimization for material extrusion polymer additive manufacturing, J. Comput. Des. Eng. 8 (2021) 979–993, http://dx.doi.org/10.1093/jcde/qwab028.
[43] A.S. Azar, M. Reiersen, E.W. Hovig, M. M'hamdi, S. Diplas, M.M. Pedersen, A novel approach for enhancing the fatigue lifetime of the components processed by additive manufacturing technologies, Rapid Prototyp. J. 27 (2021) 256–267, http://dx.doi.org/10.1108/RPJ-02-2020-0030.
[44] G. Taormina, C. Sciancalepore, M. Messori, F. Bondioli, 3D printing processes for photocurable polymeric materials: technologies, materials, and future trends, J. Appl. Biomater. Funct. Mater. 16 (3) (2018) 151–160, http://dx.doi.org/10.1177/2280800018764770.
[45] G. Lubin, Handbook of Composites, Springer Science & Business Media, 2013.
[46] S.C. Tjong, Structural and mechanical properties of polymer nanocomposites, Materials Science and Engineering: R: Reports 53 (2006) 73–197, http://dx.doi.org/10.1016/j.mser.2006.06.001.
[47] Z. Alomar, F. Concli, Compressive behavior assessment of a newly developed circular cell-based lattice structure, Mater. Des. 205 (2021) 109716, http://dx.doi.org/10.1016/j.matdes.2021.109716.
[48] O.S. Es-Said, J. Foyos, R. Noorani, M. Mendelson, R. Marloth, B.A. Pregger, Effect of layer orientation on mechanical properties of rapid prototyped samples, Mater. Manuf. Process. 15 (1) (2000) 107–122, http://dx.doi.org/10.1080/10426910008912976.
[49] S.A. Yadlapati, Influence of FDM build parameters on tensile and compression behaviors of 3D printed polymer lattice structures (Ph.D. thesis), Wright State University, 2018.
[50] W. Liu, H. Song, Z. Wang, J. Wang, C. Huang, Improving mechanical performance of fused deposition modeling lattice structures by a snap-fitting method, Mater. Des. 181 (2019) 108065, http://dx.doi.org/10.1016/j.matdes.2019.108065.
[51] N. Comand, M. Bottin, G. Rosati, One-step fast calibration of an industrial workcell, Mech. Mach. Sci. 91 (2021) 245–251, http://dx.doi.org/10.1007/978-3-030-55807-9_28.